ADVANCED ENERGY MATERIALS

www.advenergymat.de

Thick Film Polymer Solar Cells Based on Naphtho[1,2-*c*:5,6-*c*]bis[1,2,5]thiadiazole Conjugated Polymers with Efficiency over 11%

Yaocheng Jin, Zhiming Chen, Manjun Xiao, Jiajun Peng, Baobing Fan, Lei Ying, Guichuan Zhang, Xiao-Fang Jiang, Qingwu Yin, Ziqi Liang, Fei Huang,* and Yong Cao*

Two novel narrow bandgap π-conjugated polymers based on naphtho[1,2-*c*:5,6-*c*′]bis([1,2,5]thiadiazole) (NT) unit are developed, which contain the thiophene or benzodithiophene flanked with alkylthiophene as the electron-donating segment. Both copolymers exhibit strong aggregations both in solution and as thin films. The resulting copolymers with higher molecular weight show higher photovoltaic performance by virtue of the enhanced short-circuit current densities and fill factors, which can be attributed to their higher absorptivity and formation of more favorable film morphologies. Polymer solar cells (PSCs) fabricated with the copolymer PNTT achieve remarkable power conversion efficiencies (PCEs) > 11% based on both conventional and inverted structures at the photoactive layer thickness of 280 nm, which is the highest value so far observed from NT-based copolymers. Of particular interest is that the device performances are insensitive to the thickness of the photoactive layer, for which the PCEs > 10% can be achieved with film thickness ranging from 150 to 660 nm, and the PCE remains >9% at the thickness over 1 µm. These findings demonstrate that these NT-based copolymers can be promising candidates for the construction of thick film PSCs toward low-cost roll-to-roll processing technology.

1. Introduction

Polymer solar cells (PSCs) have attracted significant interest in both academia and industry because of their specific advantages for the fabrication of large-area and flexible devices.[1–5] Typically, the light harvesting layer of a PSC contains an electron-donating polymer and an electron-accepting material, which are physically blended to form a bulk-heterojunction (BHJ) structure with an interpenetrating network.[6–11] The mass production of high-performance PSCs through roll-to-roll processing technique requires the use of relatively thick films of the light-absorption layer to ensure efficient harvesting of sunlight.[12–20] However, it is challenging to optimize the trade-off between the film thickness of the photoactive layer and the power conversion efficiency (PCE).[21–23] Thicker films improve light absorption; however, the increased probability of charge recombination decreases the fill factor (FF).[24,25] In contrast, thin films have efficient charge transport, but reduced photon absorption.[26,27] Additional merits of thick film BHJ layer are that the thick film devices are less susceptible to the small defects, less sensitive to device performances, and more reproducible for processing than those devices based on thin-film BHJ layer.[28] Hence, it is necessary to develop conjugated polymers with optimized absorption profiles and high vertical hole mobility for the fabrication of thick film devices.[29,30]

Despite recent efforts toward the development of high-performance conjugated polymers for high-performance PSCs, only a few polymers can achieve PCEs greater than 10%, based on film thickness greater than 300 nm.[12,13,15,31–35] A representative class of these conjugated polymers are those comprising fluorinated aromatic species, such as 5,6-difluorobenzo[2,1,3]thiadiazole,[12–14,29] as the electron-accepting unit. In these polymers, the fluorine atoms in the backbone enhance the intramolecular and intermolecular interactions. Another case consists of conjugated polymers containing the electron-withdrawing naphtho[1,2-*c*:5,6-*c*′]bis[1,2,5]thiadiazole (NT) unit,[15,31,32,36] which has enlarged planarity, and exhibits extended absorption profiles and significantly enhanced charge carrier mobility relative to its benzo[2,1,3]thiadiazole counterpart.[37] By integrating the high-mobility centrosymmetric segment of 2,5-bis(3-alkylthiophen-2-yl)thieno[3,2-*b*]thiophene (BTTT) with an NT unit, the resulting copolymer NT812 exhibits PCEs greater than 10% in devices based on both conventional and inverted device architectures processed using either chlorinated or nonchlorinated xylenes.[31]

Y. Jin, Z. Chen, M. Xiao, B. Fan, Prof. L. Ying, G. Zhang, Dr. X.-F. Jiang, Q. Yin, Prof. F. Huang, Prof. Y. Cao
Institute of Polymer Optoelectronic Materials and Devices
State Key Laboratory of Luminescent Materials and Devices
South China University of Technology
Guangzhou 510640, P. R. China
E-mail: msleiying@scut.edu.cn; msfhuang@scut.edu.cn
J. Peng, Prof. Z. Q. Liang
Department of Materials Science
Fudan University
Shanghai 200433, P. R. China
The ORCID identification number(s) for the author(s) of this article can be found under https://doi.org/10.1002/aenm.201700944.

DOI: 10.1002/aenm.201700944

 © 2017 WILEY-VCH Verlag GmbH & Co. KGaA, Weinheim

To develop copolymers that can be used for the fabrication of thick-film devices, here we developed two novel NT-based copolymers: PNTT and PNTBDT. These copolymers were constructed by integrating NT with the electron-donating species of either thiophene (T)- or benzodithiophene (BDT)-flanked alkyl-thiophene segments, respectively, where the 2,5-linked thiophene unit resulted in kinked molecular geometry, and the BDT unit exhibited relatively weak electron-donating capability.[38] These factors resulted in decreased highest occupied molecular orbital (HOMO) energy levels, and therefore increased the open-circuit voltage (V_{OC}) with respect to the previously reported NT-based copolymer NT812.[31] Moreover, the resulting copolymers exhibited beneficial absorption profiles, strong intermolecular interactions, high hole mobility in the blend film with [6,6]-Phenyl-C71-butyric acid methyl ester ($PC_{71}BM$), and favorable phase separation when blended with $PC_{71}BM$. After careful optimization of the molecular weight, PCEs of 11.3 and 10.0% were observed for single-junction PSCs based on PNTT and PNTBDT, respectively. Importantly, the PCE of the PNTT-based device remained greater than 10% with film thicknesses of up to 660 nm, and greater than 9% with film thicknesses of up to 1050 nm. To our knowledge, these observed PCEs are among the highest values that can be attained using thick film devices,[10,11,31,39–41] which indicates the significant potential of the developed conjugated polymers for the mass production of PSCs through roll-to-roll processing.

2. Results and Discussion

2.1. Synthesis and Characterization

The molecular structures of PNTT and PNTBDT are shown in **Figure 1**a,b. The copolymers were synthesized by palladium-catalyzed Stille copolymerization of either 2,5-bis(trimethylstannyl)thiophene (Th-Sn_2) or 2,6-bis(trimethylstannyl)benzo[1,2-*b*:4,5-*b*′]dithiophene (BDT-Sn_2) monomers with distannylated 5,10-bis(5-bromo-4-(2-octyldodecyl)thiophen-2-yl)naphtho[1,2-c:5,6-c′]bis([1,2,5]thiadiazole) (see Scheme S1, Supporting Information). By controlling the polymerization time, three batches of each copolymer were afforded, with different molecular weights. The number average molecular weight (M_n) and polydispersity of these polymers were evaluated using gel permeation chromatography at 150 °C using 1,3,5-trichlorobenzene as the eluent (Figure S1, Supporting Information). The resulting copolymers with low (L), medium (M), and high (H)

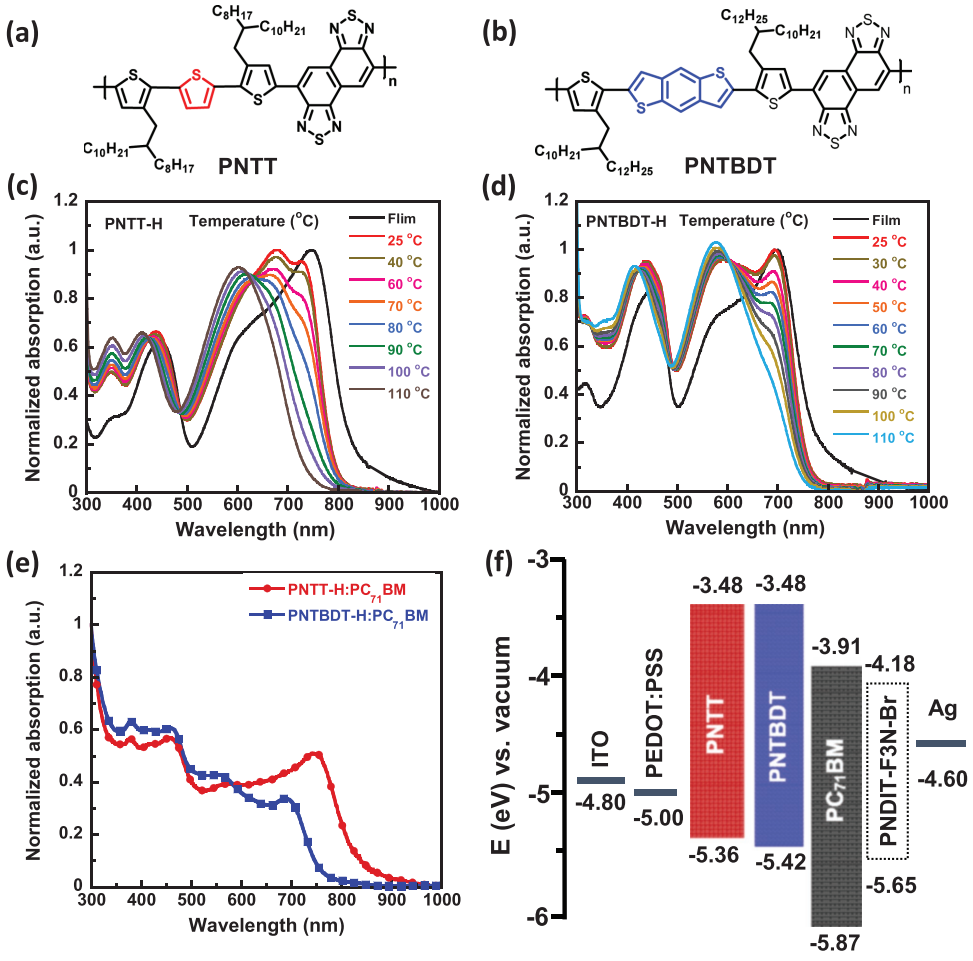

Figure 1. Molecular structures of a) PNTT and b) PNTBDT, UV–vis spectra of c) PNTT-H and d) PNTBDT-H at various temperatures in chlorobenzene (CB) solution and as thin films, e) UV–vis spectra of PNTT-H:$PC_{71}BM$ and PNTBDT-H:$PC_{71}BM$ blend films, and f) energy level alignment of materials.

© 2017 WILEY-VCH Verlag GmbH & Co. KGaA, Weinheim

M_n values of 43.4, 60.5, and 90.1 kDa, respectively, are denoted as PNTT-L, PNTT-M, and PNTT-H. On the other hand, PNTBDT copolymers with M_n values of 16.9, 32.1, and 37.1 kDa are denoted as PNTBDT-L, PNTBDT-M, and PNTBDT-H, respectively. The polydispersity of all of the copolymers was in the range of 1.7–2.1. The thermal decomposition temperatures (defined as 5% weight loss) were higher than 440 °C for all of the polymers, as determined by thermal gravimetric analysis (Figure S2a, Supporting Information). No reliable thermal transition temperatures were recorded up to 300 °C in the differential scanning calorimetry measurements (Figure S2b, Supporting Information).

2.2. Optical and Electrochemical Properties

UV–vis absorption measurements indicated that all of the copolymers exhibited dual characteristics, with a high energy band at about 440–500 nm corresponding to the π–π^* transition of the polymer backbone, and a low energy band at 500–800 nm that can be correlated with their intramolecular charge transfer characteristics (Figure 1c for PNTT-H, and Figure 1d for PNTBDT-H). As shown in Figure 1c, for PNTT-H, when the temperature was increased from 25 to 110 °C, the low-energy absorption 0-0 peak at 731 nm disappeared, and the 0-1 peak at 680 nm progressively blue-shifted to 600 nm. Moreover, the maximum absorption peak of PNTT-H at 747 nm (as thin film) was red-shifted relative to that of 680 nm observed in chlorobenzene (CB) solution (at 25 °C) with a concentration of about 1×10^{-5} g mL^{-1} (Figure 1c). In contrast, for PNTBDT-H (Figure 1d), the maximum absorption of 697 nm in the thin film was very comparable with that of 693 nm in CB solution at 25 °C; this peak gradually decreased with increasing temperature from 25 to 110 °C. These observations imply that strong aggregation of polymer chains occurred in low-temperature CB solutions and in thin films. The optical bandgaps (E_g^{opt}) of PNTT and PNTBDT, as estimated from the onsets of the thin films, are 1.42 and 1.52 eV, respectively. The PNTT:$PC_{71}BM$ blend film exhibited broader absorption than PNTBDT:$PC_{71}BM$, which is consistent with the lower bandgap of PNTT. Additionally, the molecular weights of these copolymers had significant effects on the absorption coefficients of the thin films. The polymers with lower molecular weights exhibited significantly lower absorptivity than their high molecular weight counterparts (Figure S3, Supporting Information).

Density functional theory (DFT) calculations conducted using Gaussian 09 software with the B3LYP/6-31G (d, p) basis set were performed to simulate molecular geometry and molecular orbitals.[42] The trimmers of the repeating units of copolymers, $(NTT)_3$ and $(NTBDT)_3$, were used as the model compounds. $(NTT)_3$ and $(NTBDT)_3$ exhibited kinked and zig-zag geometry, respectively, and both of them were planar from the side view. The lowest unoccupied molecular orbitals (LUMOs) of the model compounds were comparable. $(NTBDT)_3$ was found to have a slightly lower HOMO level than that of $(NTT)_3$, which was attributed to the more delocalized electron distribution in the central phenyl unit of BDT (Figure S4, Supporting Information). The frontier orbital levels of the copolymers were evaluated by cyclic voltammetry (CV), using tetra-*n*-butylammonium hexafluorophosphate (0.1 M in acetonitrile) as the electrolyte, a saturated calomel electrode as the reference electrode, and graphite as the working electrode. The measured HOMO/LUMO levels of PNTT-H and PNTBDT-H are –5.36/–3.48 and –5.42/–3.48 eV, respectively (Figure S5, Supporting Information). The slightly deeper HOMO of PNTBDT-H would lead to slightly higher V_{OC} of the resulting devices as the V_{OC} is proportional to the difference between the HOMO energy level of the donor and the LUMO of the electron-acceptor.

2.3. Photovoltaic Performance

The photovoltaic performance of the copolymers was evaluated based on PSCs with the following structure: ITO/PEDOT:PSS/copolymer:$PC_{71}BM$/PNDIT-F3N-Br/Ag. A water/alcohol soluble poly[(9,9-bis(3′-((*N*,*N*-dimethyl)-*N*-ethylammonium)propyl)-2,7-fluorene)-*alt*-5,5′-bis(2,2′-thiophene)-2,6-naphthalene-1,4,5,8-tetracaboxylic-*N*,*N*′-di(2-ethylhexyl)imide]dibromide (PNDIT-F3N-Br) layer was deposited onto the photoactive layer to facilitate electron collection.[43] Our initial optimization of devices is performed by screening the weight ratio of donor to acceptor, processing solvent, temperature of the substrate, thermal annealing of the fabricated bulk-heterojunction films, and the processing solvent additives. The observed current density–voltage (*J*–*V*) curves of devices under simulated AM 1.5 G irradiation with intensity of 100 mW cm^{-2} are shown in Figures S6–S10 (Supporting Information) with relevant photovoltaic parameters summarized in Tables S1–S5 (Supporting Information). It is worth mentioning that the device performances are rather sensitive to the substrate temperature, for which the device based on BHJ film processed at 100 °C presents the highest PCE (Figure S8 and Table S3, Supporting Information). The detailed photovoltaic parameters of the resulting devices based on copolymers with various molecular weights are summarized in **Table 1**, and the *J*–*V* characteristics and external quantum efficiency (EQE) spectra are illustrated in **Figure 2**.

The optimized device based on PNTT-L exhibited a moderate PCE of 6.0%, with an open-circuit voltage (V_{OC}) of 0.77 V, a short circuit current (J_{SC}) of 12.0 mA cm^{-2}, and a FF of 64.5%. A slightly improved PCE of 7.2% was observed using PNTT-M because of its improved J_{SC} (14.4 mA cm^{-2}) and FF (71.6%). The device fabricated using high molecular weight PNTT-H exhibited an excellent PCE of 11.3% (V_{OC} = 0.77 V, J_{SC} = 20.5 mA cm^{-2}, and FF = 71.6%). In addition, the device based on an inverted architecture, ITO/ZnO/PNTT-H:$PC_{71}BM$/MoO_3/Al, also exhibited a high PCE (11.1%) (V_{OC} = 0.75 V, J_{SC} = 20.7 mA cm^{-2}, and FF = 71.5%). The corresponding *J*–*V* and EQE curves are shown in Figure S11 (Supporting Information). To our knowledge, the PCEs greater than 11% observed from both normal and inverted structures are the highest values so far observed from a single junction PSC using an NT-based copolymer as the electron-donating material.[30–32] Of particular importance is that the resulting PNTT devices exhibited remarkable stability, for which the PCE slightly decreased from 10.8 to 10.4% after 144 h (6 days, Figure S12 and Table S6, Supporting Information), and the PCE slightly decreased from 11.3 to 10.2% (Figure S13 and Table S7, Supporting Information) after continuous illumination for 12 h under AM 1.5 G

© 2017 WILEY-VCH Verlag GmbH & Co. KGaA, Weinheim

Table 1. Molecular weight of polymers and photovoltaic parameters measured under AM 1.5G, 100 mW cm^{-2} illumination.

Polymer	M_n [kDa]	PDI	V_{OC} [V]	J_{sc} [mA cm^{-2}]	FF [%]	PCE$_{max}$ [Avg.][a)] [%]	Thickness [nm]
PNTT-L	43.4	2.1	0.77	12.0 ± 0.8	64.5 ± 0.8	6.0 (5.8)	280
PNTT-M	60.5	1.9	0.77	14.4 ± 1.3	65.3 ± 0.6	7.2 (7.0)	280
PNTT-H	90.1	1.7	0.77	20.2 ± 0.8	71.8 ± 0.1	11.3 (11.1)	280
PNTBDT-L	16.9	1.7	0.86	8.2 ± 0.4	60.8 ± 1.6	4.3 (4.2)	300
PNTBDT-M	32.1	1.7	0.85	14.7 ± 0.9	67.9 ± 0.7	8.4 (8.3)	300
PNTBDT-H	37.1	1.8	0.84	16.5 ± 1.2	72.1 ± 1.4	10.0 (9.9)	300

[a)]The PCE values in the bracket represent the average values of 15 devices. Device structure: ITO/PEDOT:PSS/polymer:$PC_{71}BM$ (1:1.5 wt:wt)/PNDIT-F3N-Br/Ag.

at 100 mW cm^{-2}. Furthermore, a similar trend of molecular weight versus PCE was observed when using PNTBDT in the light-harvesting layer of PSCs with conventional structures. The devices fabricated using PNTBDT-L and PNTBDT-M exhibit moderate PCEs of 4.3 and 8.4%, respectively. PNTBDT-H-based device shows a significantly increased PCE, to 10.0% (V_{OC} = 0.84 V, J_{SC} = 16.5 mA cm^{-2}, and FF = 72.1%). These findings indicate that molecular weight played a critical role in achieving high photovoltaic performance.

The slightly higher V_{OC} of the PNTBDT-H-based device, relative to that of the PNTT-H-based device, agreed with its deeper HOMO energy level. Additionally, the hole mobility of the PNTT-H:$PC_{71}BM$ blend film, determined using the space-charge limited current (SCLC) method, was estimated to be 3.3×10^{-3} cm^2 V^{-1} s^{-1}, comparable with that of the PNTBDT-H:$PC_{71}BM$ blend film (2.8×10^{-3} cm^2 V^{-1} s^{-1}; Figure S14, Supporting Information). We also used the dark- and photo-charge extraction by linearly increasing voltage (CELIV) method to measure the charge carrier mobility (Figure S15 and Table S8, Supporting Information). The obtained hole mobilities of PNTT-H devices are 1.66×10^{-3} and 2.41×10^{-3} cm^2 V^{-1} s^{-1} corresponding to the photo- and dark CELIV, respectively. Under the same conditions, the PNTBDT-H devices showed comparable hole mobilities of 1.50×10^{-3} and 2.08×10^{-3} cm^2 V^{-1} s^{-1}

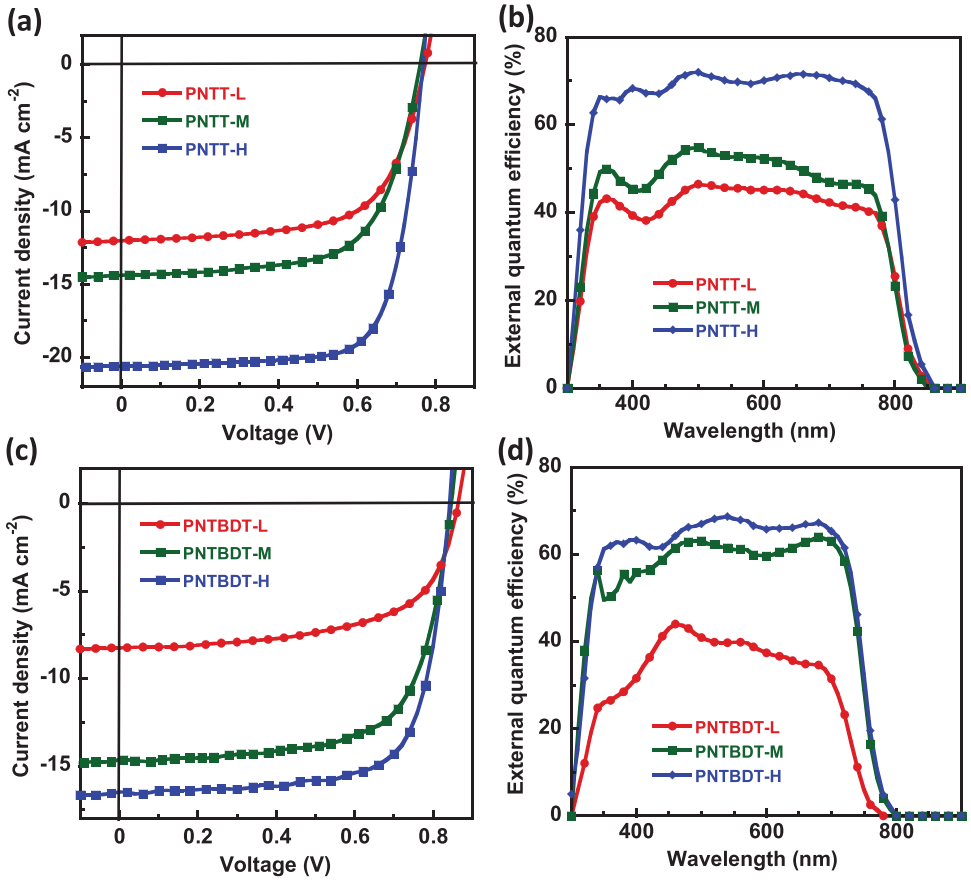

Figure 2. *J–V* and EQE characteristics of devices based on a,b) PNTT and c,d) PNTBDT with various molecular weight.

© 2017 WILEY-VCH Verlag GmbH & Co. KGaA, Weinheim

for the photo- and dark CELIV, respectively. The higher J_{SC} of the PNTT-H-based device, relative to that of the PNTBDT-H-based device, was attributed to its broader light-harvesting capability (Figure 1e). The accuracy of the observed J_{SC} values was confirmed by the EQE spectra (Figure 2b,d), which exhibited broad responses from about 300 to 800 nm. Devices based on PNTT-H and PNTBDT-H exhibited maximum values of greater than 60% in the ranges of 350–780 and 350–720 nm, respectively. The differences between the current densities integrated from the EQE spectra and those calculated from the *J–V* curves are less than 5%. In addition, we also recorded internal quantum efficiency (IQE) of the devices with best performances, with relevant spectra shown in Figure S16 (Supporting Information). One notes that the IQE values attained very high value over 80% across a wide range of 450–650 nm for PNTT; and the IQE values are higher than 70% in the range of 350–720 nm. These observations imply that these resulting copolymers might have highly efficient charge generation and extraction, and relatively weak bimolecular recombination, and thus can be used to fabricate thick-film devices.

2.4. Film Morphology

The surface topography and phase separation of BHJ films were examined using tapping-mode atomic force microscopy (AFM) and transmission electron microscopy (TEM), respectively (**Figure 3**, and Figure S17, Supporting Information). For both copolymers, molecular weight had significant effects on film morphology. The PNTT-L:$PC_{71}BM$ blend film exhibited a relatively rough surface, with obvious phase separation and granular domains across the entire film, and a root-mean-square (RMS) value of 2.81 nm (Figure 3a). In contrast, the PNTT-H:$PC_{71}BM$ blend film exhibited a smoother surface, with significantly smaller granular domains (RMS = 1.45 nm, Figure 3b), indicating the greater miscibility of PNTT with $PC_{71}BM$. In addition, the blend film based on PNTBDT-L exhibited a rougher surface (Figure 3c) than that of PNTBDT-H (Figure 3d).

The obtained TEM images clearly demonstrate the differences in the phase separation of blend films based on copolymers with different molecular weights. For example, PNTT-H:$PC_{71}BM$ (Figure 3f) exhibits a more slender fibrous structures and continuous interpenetrating features than PNTT-L:$PC_{71}BM$ (Figure 3e). These features enhanced charge carrier transport in the PNTT-H:$PC_{71}BM$ layer.[44] In addition, severe phase separation and large clusters were observed in the PNTBDT-L:$PC_{71}BM$ blend film (Figure 3g). The PNTBDT-H:$PC_{71}BM$ blend film exhibited finely distributed fibrous structures across the film (Figure 3h). These observations demonstrate that high molecular weight polymers produced more favorable film morphologies in the blend films, a finding consistent with the higher J_{SC} values of the high molecular weight samples.

2.5. Charge Transfer, Recombination, and Extraction

The charge transfer properties of the fabricated PSC devices were examined by measuring the photoluminescence (PL) spectra of copolymer:$PC_{71}BM$ blend films.[45] The high molecular weight copolymers PNTT-H and PNTBDT-H were used for this investigation because of their high photovoltaic performances. The PL spectra of both copolymers were almost completely quenched in their respective blend films (Figure S18, Supporting Information), indicating efficient charge transfer from the copolymers to $PC_{71}BM$. To investigate the charge recombination mechanisms of the fabricated devices, we

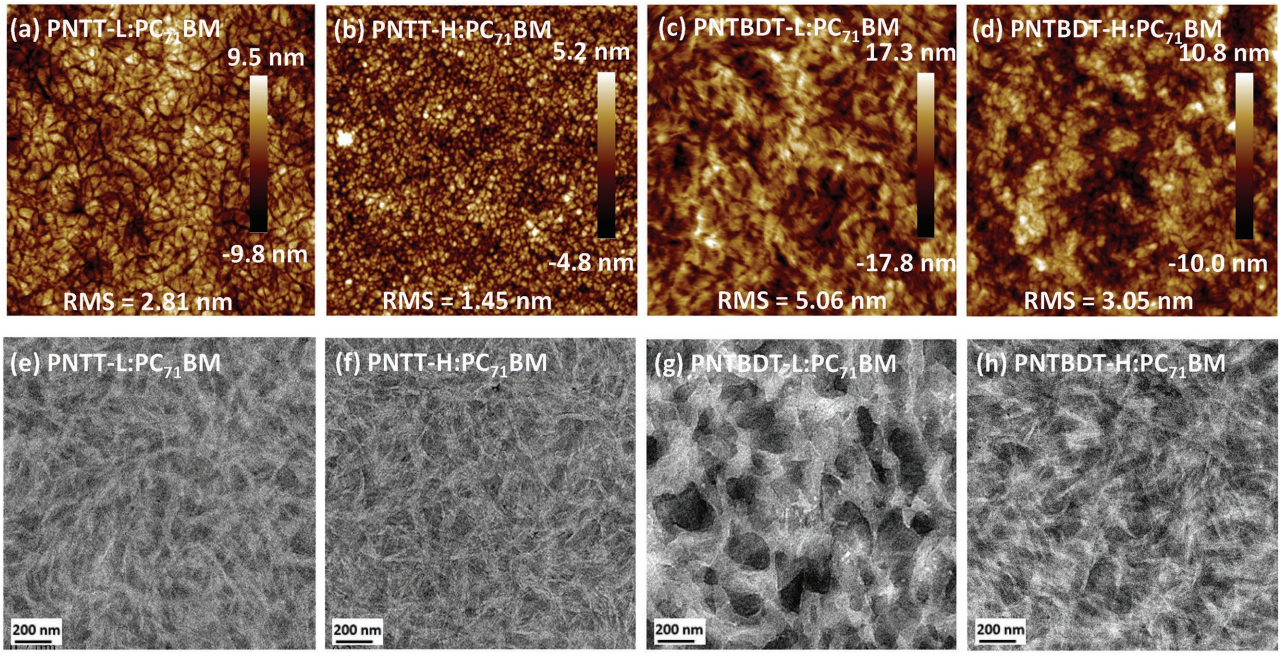

Figure 3. a–d) AFM and e–h) TEM images of a,e) PNTT-L:$PC_{71}BM$, b,f) PNTT-H:$PC_{71}BM$, c,g) PNTBDT-L:$PC_{71}BM$, and d,h) PNTBDT-H blend films.

© 2017 WILEY-VCH Verlag GmbH & Co. KGaA, Weinheim

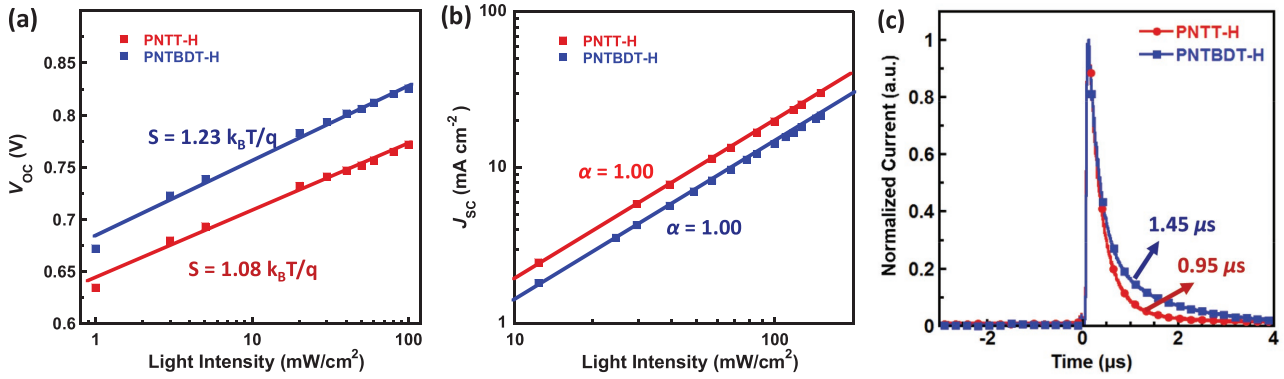

Figure 4. a) V_{OC} and b) J_{SC} as a function of light intensity, and c) transient photocurrent of PNTT-H- and PNTBDT-H-based devices.

examined the open-circuit voltage and photocurrent as a function of the natural logarithm of light intensity (**Figure 4**a,b).

The slope of a plot of V_{OC} versus log(P_{light}) provided the value of k_BT/q,[46] where k_B is the Boltzmann constant, T is the temperature (K), and q is the elementary charge. The strong dependence of V_{OC} on P_{light} resulted in greater values of k_BT/q when additional trap-assisted recombination, or similar mechanisms, were present in a device. The observed slopes of the PNTT-H- and PNTBDT-H-based devices were 1.08 and 1.23 k_BT/q, respectively (Figure 4a), indicating that the other recombination mechanisms (except for bimolecular recombination) such as trap-assisted recombination are not significant in such devices based on both PNTT-H and PNTBDT-H.[47] To further evaluate the extent of bimolecular recombination in such devices, we measured the dependence of J_{SC} on the light intensity, described as $J_{SC} \propto (P_{light})^{\alpha}$,[48] where P_{light} is the light intensity (from 12 to 150 mW cm^{-2}). We note the slope α was calculated to be 1.00 for devices based on both copolymers (Figure 4b). Since it is well established that the bimolecular recombination is weak when the exponential factor of $J_{SC} - P_{light}$ is approaching unity,[49,50] thus it is reasonable to surmise that the bimolecular recombination was weak for devices based on both copolymers. This observation was consistent with the high FF values (>70%) of the corresponding PSC devices. Furthermore, transient photocurrent (TPC)[51] measurements demonstrated that the device based on PNTT-H had an electron extraction time of 0.95 µs, shorter than that for the PNTBDT-H-based device (1.45 µs; Figure 4c). This indicated that charge carriers were more efficiently extracted from the photoactive layer of the PNTT-H-based device, which agreed with the higher J_{SC} of the PNTT-H-based device.

2.6. Thick Film Devices Based on PNTT-H

The reduced charge recombination, faster charge extraction, and relatively high hole mobility of PNTT-H enabled us to fabricate devices with a thick photoactive layer. Devices were fabricated with a conventional structure, and the thickness of the photoactive layer ranged from 150 to 1050 nm. The detailed photovoltaic parameters as a function of film thickness are plotted in **Figure 5**, and the relevant J–V characteristics and EQE spectra of devices (Figure S19, Supporting Information), and photovoltaic parameters (Table S9, Supporting Information) are provided in the Supporting Information. As shown in Figure 5, the V_{OC} is about 0.76 ± 0.01 V for all of the devices. The

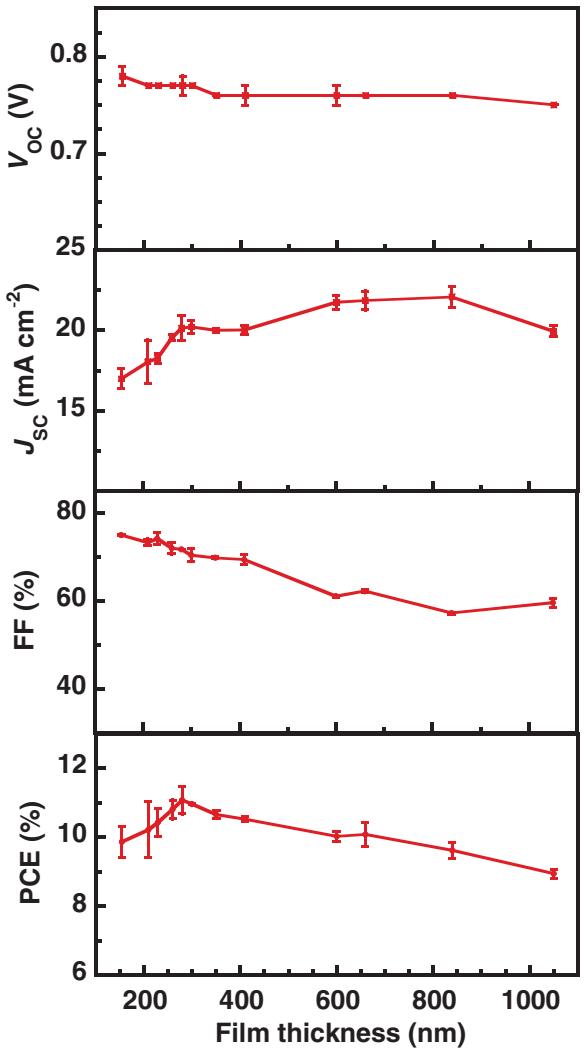

Figure 5. Photovoltaic parameters of PNTT-H-based PSCs. a) J_{SC}, b) V_{OC}, c) FF, and d) PCE versus the thickness of PNTT:$PC_{71}BM$ blend films.

© 2017 WILEY-VCH Verlag GmbH & Co. KGaA, Weinheim

J_{SC} gradually increases from 16.7 ± 0.6 to 22.1 ± 0.6 mA cm^{-2} as the film thickness increases from 150 to 840 nm, and then slowly decreases to 19.9 ± 0.6 mA cm^{-2} at a film thickness of 1050 nm. It is noted that the EQE responses gradually enhanced with the film thickness, and slightly decreased at the film thickness of 1050 nm, which are consistent with those values observed from the *J–V* measurements. The combination of the observed EQE and the UV–vis spectra under various film thickness indicated efficient charge collection of these resulting devices, which is consistent with the relatively short charge extraction time. The FF value is greater than 70% with film thicknesses of up to 300 nm, and depletes to 59.6 ± 1.0% with a film thickness of 1050 nm. The combination of these photovoltaic parameters resulted in PCEs greater than 10% with film thicknesses of 150–660 nm, which remained greater than 9% at a film thickness of 1050 nm. The insensitive PCE regarding to the film thickness is understandable because of the trade-off between light-harvesting capability and charge carrier transport in the BHJ films. Despite the thicker films can absorb sunlight more efficiently (Figure S20a, Supporting Information) that can lead to enhanced J_{SC} and thus enhanced PCE, the hole mobility slightly decreased with the increase of film thickness (Figure S20b and Table S10, Supporting Information) that will lead to the slightly decreased J_{SC} and FF that can result in decreased PCE. The combination of these effects results in the slightly decreased PCE with the increase of film thickness. It is also worth pointing out that the film thickness does not show significant effects on the bimolecular recombination as the dependence of photocurrent on the light intensity at various film thickness are quite similar (Figure S20c, Supporting Information). To our knowledge, this is the highest PCE observed from so far reported single-junction PSCs with a BHJ film thickness of 1 µm.[10,11,31,36–38] The insensitivity of PCE to film thickness is of particular importance for the mass production of PSCs using high-throughput roll-to-roll techniques.

3. Conclusion

In summary, we developed two novel π-conjugated polymers, PNTT and PNTBDT, containing naphtho[1,2-*c*:5,6-*c*]bis[1,2,5]thiadiazole units. Both of these polymers exhibit deep HOMO energy levels and high hole mobilities. Their molecular weights had significant effects on the morphologies of the BHJ films and photovoltaic performance. Devices based on copolymers with high molecular weights exhibited high PCEs of greater than 10%, which was attributed to weak bimolecular recombination. The devices fabricated using PNTT-H:$PC_{71}BM$ as the photoactive layer, based on both conventional and inverted architectures, exhibited PCEs greater than 11%, which are the highest values so far observed using NT-based copolymers. Furthermore, PSCs based on PNTT-H exhibited PCEs greater than 10% with photoactive layer thicknesses of 150–660 nm and a PCE of 9% with a film thickness of 1050 nm. This was the highest PCE observed from a single-junction PSC with a BHJ film thickness of 1 µm. These results demonstrated that the novel NT-based conjugated polymers were promising candidates for the mass production of high-performance PSCs.

Supporting Information

Supporting Information is available from the Wiley Online Library or from the author.

Acknowledgements

This work was financially supported by the Ministry of Science and Technology of China (Grant No. 2014CB643501) and the National Natural Science Foundation of China (Grant Nos. 91633301, 51673069, and 21520102006).

Conflict of Interest

The authors declare no conflict of interest.

Keywords

high-performance solar cells, naphtho[1,2-*c*:5,6-*c*]bis[1,2,5]thiadiazole, polymer solar cells, thick-film devices

Received: April 6, 2017
Revised: June 19, 2017
Published online:

[1] L. Lu, T. Zheng, Q. Wu, A. M. Schneider, D. Zhao, L. Yu, *Chem. Rev.* **2015**, *115*, 12666.
[2] L. Liu, G. Zhang, B. He, F. Huang, *Chin. J. Chem.* **2015**, *33*, 902.
[3] Y.-J. Cheng, S.-H. Yang, C.-S. Hsu, *Chem. Rev.* **2009**, *109*, 5868.
[4] C. C. Chen, W. H. Chang, K. Yoshimura, K. Ohya, J. You, J. Gao, Z. Hong, Y. Yang, *Adv. Mater.* **2014**, *26*, 5670.
[5] J. Huang, J. H. Carpenter, C. Z. Li, J. S. Yu, H. Ade, A. K. Jen, *Adv. Mater.* **2016**, *28*, 967.
[6] L. Liu, G. Zhang, B. He, S. Liu, C. Duan, F. Huang, *Mater. Chem. Front.* **2017**, *1*, 499.
[7] Z. Li, X. Xu, W. Zhang, X. Meng, W. Ma, A. Yartsev, O. Inganas, M. R. Andersson, R. A. Janssen, E. Wang, *J. Am. Chem. Soc.* **2016**, *138*, 10935.
[8] J. Y. Yuan, H. L. Dong, M. Li, X. D. Huang, J. Zhong, Y. Y. Li, W. L. Ma, *Adv. Mater.* **2014**, *26*, 3624.
[9] B. Kan, M. Li, Q. Zhang, F. Liu, X. Wan, Y. Wang, W. Ni, G. Long, X. Yang, H. Feng, *J. Am. Chem. Soc.* **2015**, *137*, 3886.
[10] H.-C. Liao, C.-C. Ho, C.-Y. Chang, M.-H. Jao, S. B. Darling, W.-F. Su, *Mater. Today* **2013**, *16*, 326.
[11] Y. Lin, J. Wang, Z. G. Zhang, H. Bai, Y. Li, D. Zhu, X. Zhan, *Adv. Mater.* **2015**, *27*, 1170.
[12] S. C. Price, A. C. Stuart, L. Yang, H. Zhou, W. You, *J. Am. Chem. Soc.* **2011**, *133*, 4625.
[13] X. Hu, C. Yi, M. Wang, C. H. Hsu, S. Liu, K. Zhang, C. Zhong, F. Huang, X. Gong, Y. Cao, *Adv. Energy. Mater.* **2014**, *4*, 1400378.
[14] L. Nian, Z. Chen, S. Herbst, Q. Li, C. Yu, X. Jiang, H. Dong, F. Li, L. Liu, F. Würthner, J. Chen, Z. Xie, Y. Ma, *Adv. Mater.* **2016**, *28*, 7521.
[15] Y. Liu, J. Zhao, Z. Li, C. Mu, W. Ma, H. Hu, K. Jiang, H. Lin, H. Ade, H. Yan, *Nat. Commun.* **2014**, *5*, 5293.
[16] J. Zhao, Y. Li, G. Yang, K. Jiang, H. Lin, H. Ade, W. Ma, H. Yan, *Nat. Energy* **2016**, *1*, 15027.
[17] V. Vohra, K. Kawashima, T. Kakara, T. Koganezawa, I. Osaka, K. Takimiya, H. Murata, *Nat. Photonics* **2015**, *9*, 403.

 © 2017 WILEY-VCH Verlag GmbH & Co. KGaA, Weinheim

[18] Q. Fan, W. Su, X. Guo, B. Guo, W. Li, Y. Zhang, K. Wang, M. Zhang, Y. Li, *Adv. Energy Mater.* **2016**, *6*, 1600430.
[19] S. J. Ko, B. Walker, T. L. Nguyen, H. Choi, J. Seifter, M. A. Uddin, T. Kim, S. Kim, J. Heo, G. H. Kim, *Adv. Funct. Mater.* **2016**, *26*, 3324.
[20] X. Zhu, B. Xia, K. Lu, H. Li, R. Zhou, J. Zhang, Y. Zhang, Z. Shuai, Z. Wei, *Chem. Mater.* **2016**, *28*, 943.
[21] X. Yang, C.-C. Chueh, C.-Z. Li, H.-L. Yip, P. Yin, H. Chen, W.-C. Chen, A. K. Y. Jen, *Adv. Energy Mater.* **2013**, *3*, 666.
[22] L. Ye, S. Zhang, W. Zhao, H. Yao, J. Hou, *Chem. Mater.* **2014**, *26*, 3603.
[23] C. Cabanetos, A. El Labban, J. A. Bartelt, J. D. Douglas, W. R. Mateker, J. M. Fréchet, M. D. McGehee, P. M. Beaujuge, *J. Am. Chem. Soc.* **2013**, *135*, 4656.
[24] W. Li, K. H. Hendriks, W. Roelofs, Y. Kim, M. M. Wienk, R. A. Janssen, *Adv. Mater.* **2013**, *25*, 3182.
[25] L. Huo, T. Liu, B. Fan, Z. Zhao, X. Sun, D. Wei, M. Yu, Y. Liu, Y. Sun, *Adv. Mater.* **2015**, *27*, 6969.
[26] K. Sun, Z. Xiao, S. Lu, W. Zajaczkowski, W. Pisula, E. Hanssen, J. M. White, R. M. Williamson, J. Subbiah, J. Ouyang, *Nat. Commun.* **2015**, *6*, 6013.
[27] D. Liu, Q. Zhu, C. Gu, J. Wang, M. Qiu, W. Chen, X. Bao, M. Sun, R. Yang, *Adv. Mater.* **2016**, *28*, 8490.
[28] C. Duan, F. Huang, Y. Cao, *Polym. Chem.* **2015**, *6*, 8081.
[29] J. A. Bartelt, D. Lam, T. M. Burke, S. M. Sweetnam, M. D. McGehee, *Adv. Energy Mater.* **2015**, *5*, 1500577.
[30] C. M. Proctor, J. A. Love, T. Q. Nguyen, *Adv. Mater.* **2014**, *26*, 5957.
[31] Z. Chen, P. Cai, J. Chen, X. Liu, L. Zhang, L. Lan, J. Peng, Y. Ma, Y. Cao, *Adv. Mater.* **2014**, *26*, 2586.
[32] H. Hu, K. Jiang, G. Yang, J. Liu, Z. Li, H. Lin, Y. Liu, J. Zhao, J. Zhang, F. Huang, Y. Qu, W. Ma, H. Yan, *J. Am. Chem. Soc.* **2015**, *137*, 14149.
[33] K. Kawashima, T. Fukuhara, Y. Suda, Y. Suzuki, T. Koganezawa, H. Yoshida, H. Ohkita, I. Osaka, K. Takimiya, *J. Am. Chem. Soc.* **2016**, *138*, 10265.
[34] Y. Jin, Z. Chen, S. Dong, N. Zheng, L. Ying, X.-F. Jiang, F. Liu, F. Huang, Y. Cao, *Adv. Mater.* **2016**, *28*, 9811.
[35] J. Lee, D. H. Sin, B. Moon, J. Shin, H. G. Kim, M. Kim, K. Cho, *Energy Environ. Sci.* **2017**, *10*, 247.
[36] I. Osaka, K. Takimiya, *Adv. Mater.* **2017**, *29*, 1605218.
[37] M. Wang, X. Hu, P. Liu, W. Li, X. Gong, F. Huang, Y. Cao, *J. Am. Chem. Soc.* **2011**, *133*, 9638.
[38] H. Yao, L. Ye, H. Zhang, S. Li, S. Zhang, J. Hou, *Chem. Rev.* **2016**, *116*, 7397.
[39] L. Zeng, C. W. Tang, S. H. Chen, *Appl. Phys. Lett.* **2010**, *97*, 053305.
[40] I. Osaka, M. Saito, T. Koganezawa, K. Takimiya, *Adv. Mater.* **2014**, *26*, 331.
[41] S. J. Ko, B. Walker, T. L. Nguyen, H. Choi, J. Seifter, M. A. Uddin, T. Kim, S. Kim, J. Heo, G. H. Kim, *Adv. Funct. Mater.* **2016**, *26*, 3324.
[42] M. J. Frisch, G. W. Trucks, H. B. Schlegel, G. E. Scuseria, M. A. Robb, J. R. Cheeseman, G. Scalmani, V. Barone, B. Mennucci, G. A. Petersson, H. Nakatsuji, M. Caricato, X. Li, H. P. Hratchian, A. F. Izmaylov, J. Bloino, G. Zheng, J. L. Sonnenberg, M. Hada, M. Ehara, K. Toyota, R. Fukuda, J. Hasegawa, M. Ishida, T. Nakajima, Y. Honda, O. Kitao, H. Nakai, T. Vreven, J. A. Montgomery Jr., J. E. Peralta, F. Ogliaro, M. Bearpark, J. J. Heyd, E. Brothers, K. N. Kudin, V. N. Staroverov, R. Kobayashi, J. Normand, K. Raghavachari, A. Rendell, J. C. Burant, S. S. Iyengar, J. Tomasi, M. Cossi, N. Rega, J. M. Millam, M. Klene, J. E. Knox, J. B. Cross, V. Bakken, C. Adamo, J. Jaramillo, R. Gomperts, R. E. Stratmann, O. Yazyev, A. J. Austin, R. Cammi, C. Pomelli, J. W. Ochterski, R. L. Martin, K. Morokuma, V. G. Zakrzewski, G. A. Voth, P. Salvador, J. J. Dannenberg, S. Dapprich, A. D. Daniels, O. Farkas, J. B. Foresman, J. V. Ortiz, J. Cioslowski, D. J. Fox, Gaussian, Inc., Wallingford CT, Gaussian 09, Revision A.02, **2009**.
[43] Z. Wu, C. Sun, S. Dong, X.-F. Jiang, S. Wu, H. Wu, H.-L. Yip, F. Huang, Y. Cao, *J. Am. Chem. Soc.* **2016**, *138*, 2004.
[44] T. Liu, X. Pan, X. Meng, Y. Liu, D. Wei, W. Ma, L. Huo, X. Sun, T. H. Lee, M. Huang, H. Choi, J. Y. Kim, W. C. H. Choy, Y. Sun, *Adv. Mater.* **2017**, *29*, 1604251.
[45] J. Subbiah, B. Purushothaman, M. Chen, T. Qin, M. Gao, D. Vak, F. H. Scholes, X. Chen, S. E. Watkins, G. J. Wilson, A. B. Holmes, W. W. H. Wong, D. J. Jones, *Adv. Mater.* **2015**, *27*, 702.
[46] L. Lu, W. Chen, T. Xu, L. Yu, *Nat. Commun.* **2015**, *6*, 7327.
[47] J. Min, X. Jiao, I. Ata, A. Osvet, T. Ameri, P. Bäuerle, H. Ade, C. J. Brabec, *Adv. Energy Mater.* **2016**, *6*, 1502579.
[48] S. R. Cowan, A. Roy, A. J. Heeger, *Phys. Rev. B* **2010**, *82*, 245207.
[49] A. K. Kyaw, D. H. Wang, D. Wynands, J. Zhang, T. Q. Nguyen, G. C. Bazan, A. J. Heeger, *Nano Lett.* **2013**, *13*, 3796.
[50] M. Mandoc, F. Kooistra, J. Hummelen, B. De Boer, P. Blom, *Appl. Phys. Lett.* **2007**, *91*, 263505.
[51] C. J. Brabec, N. S. Sariciftci, J. C. Hummelen, *Adv. Funct. Mater.* **2011**, *11*, 15.

© 2017 WILEY-VCH Verlag GmbH & Co. KGaA, Weinheim